# Combined Finite–Discrete element method for parameter identification of masonry structures

R. Bravo[a], J.L. Pérez–Aparicio[b]

[a] *University of Granada, Department of Structural Mechanics and Hydraulic Engineering. Campus de Fuentenueva s/n., Granada, 18071, Spain*
[b] *Universitat Politècnica València, Department of Continuum Mechanics & Structures. Camino de Vera s/n, Valencia, 46022, Spain*

**Abstract**

Masonry structures are constructions made of discontinuous blocks that require unique numerical methods incorporating contact, friction, and cohesion models for their analysis. Given the large number of aging structures of this type still in use, there is a demand to combine these numerical methods with optimization algorithms to help in structural health monitoring. This paper combines discrete and finite methods with genetic algorithms for parametrizing two masonry structures. The first is a bridge with a large number of blocks, the material properties of which are estimated with a small error. Since the loads are low, the mortar's properties are irrelevant. The second is a buried ogival vault; starting from only four pieces of experimental data from the literature and related with the failure loads, the material and contact properties are calculated. From them, many other failure loads are again iteratively calculated and favorably compared with the rest of the data. To further validate the inverse problem, the computed properties are used for several runs of the same vault but under different loads, obtaining again an almost perfect agreement with the experiments.

*Keywords:* Masonry structures, Combined Finite–Discrete element method, Genetic algorithm, Inverse problem, Parameter identification

## 1. Introduction

The masonry bridge is the most ancient structural typology in the history of humanity that has reached our days due to its excellent durability, a consequence of the high stiffness and strength of stones, [1]; in addition, its geometry produces only internal compressive forces, without tractions. Hence, a great legacy of masonry bridges currently in service must be maintained and preserved. Most of these bridges were built during the last two centuries due to the birth and subsequent growth of road and rail transport, [2, 3]. In the last decades, new demands on higher speeds and loads, especially from locomotives, railcars, or heavy traffic, have made it necessary to verify their structural capacity using computational tools capable of detecting the partially degraded mechanical parameters.

The structural behavior of masonry is highly nonlinear due to its inner discontinuous nature, composed of stone or brick blocks that interact by friction and contact. These interactions are the key to the stability of the structure and its static and dynamic response. Many approaches have been undertaken to analyze the behavior of masonry arches: from Vitruvius [4] in the first century B.C. to the graphic methods of the XIX century [5], but in general not taking into account the internal discontinuous behavior. Later, semi–empirical methods from the report [6] or with linear and nonlinear elasticity [7] emerged in the XX century. However, these methods are only suitable for very simple structures with behavior that can be considered linear.

For analyzing the mechanical response of systems composed of discontinuous blocks or particles, advanced computational methods such as the Discrete Element Method (DEM), [8], were developed in the late years of the 1970 decade. DEM is a numerical tool initially conceived for soil mechanics and geotechnical applications. Their responses result from multiple interactions due to contact and friction; these contacts are among rigid or elastic bodies, initially soil particles or rocks. The similarities between the behavior of rocks and masonry made the extension of DEM to the latter straightforward. Therefore, DEM has already been applied to masonry for relatively simple geometries, such as static analysis of arches [9] although under several loading configurations [10]. Increased computation capabilities have allowed it to extend DEM to complex two– and three–dimensional structures such as buildings and domes under static and dynamic regimes: [11, 12, 13]. An alternative to analyzing masonry is utilizing the discrete macro–element approach [14]. However, its ability to represent internal strain fields is limited.

Parallel to the development of DEM, the NSCD method from [15] and the Finite Element Method (FEM) with contact interfaces [16] were formulated for problems involving interactions between rigid/elastic bodies. However, their application requires very high computational cost making them less advantageous. The DEM is appropriate for analyzing problems focused on precisely representing kinematics and interactions between bodies. However, its accuracy for calculating deformations/stresses inside an elastic body is inferior to that of the FEM, [17].

To overcome these limitations, DEM and FEM have been coupled to analyze contact interactions and internal elasticity, respectively, with a reasonable computational cost. The outcome is the combined Finite–Discrete Element Method (Fem-

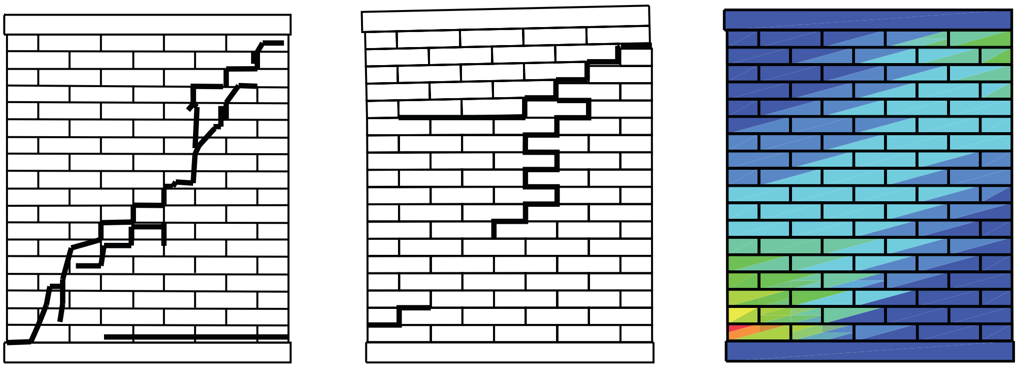

Figure 1: For prescribed displacement 1.5 [mm] at the top of the wall: experimental crack progress, left; FemDem crack progress, center; Tresca stress, right; red maximum of 3.43 [MPa] with a blue minimum of 0.

Dem) of [18], a numerical tool widely used in recent years in the field of rock and geomechanics, [19]. FemDem is also advantageous for the analysis of masonry structures to overcome the above limitations, as shown in the collapse analysis of static [20] or of dynamic [21, 22, 23] walls and arches.

Masonry structures were primarily built in times without scientific structural knowledge but with a deep inherited constructive background. As mentioned, it is essential to quantify the mechanical parameters of the structures for their preservation. Several techniques have been developed to identify mechanical parameters based on minor destructive tests based on localized extraction of small samples [24]. But often, it is difficult to access the areas of interest of the structure, or due to special conservation restrictions; the extraction is prohibited. To overcome this drawback, advanced non–destructive techniques allow proper monitoring of mechanical parameters. Installing monitoring systems on masonry bridges makes it possible to follow the parameter evolution and detect structural problems, which may lead to masonry damage or collapse, [25].

The information provided by the monitoring system (displacements, accelerations, vibration frequencies...) can be complemented with FEM simulations using an inverse problem for a correct analysis and decision–making of the structural health of the masonry bridge [26]. However, as argued before, FEM does not consider the discontinuous nature of masonry. Therefore, processing the information with a numerical method, such as FemDem, able to model discontinuities is necessary. In addition, replacing sensor measurements with a numerical simulation is a valid strategy to provide initial data for a FemDem–based inverse problem in theoretical developments. This methodology provides qualitative insight into the future ability of the inverse problem to detect mechanical parameters and automatically detect possible defects.

DEM has been used outside structural mechanics in combination with inverse/optimization algorithms for micro–parameter calibration of granular and cemented materials, [27, 28], and the optimization of the shape of bucket elevators, [29]. But at this time, and as far as we know, the application of DEM or FemDem to identify mechanical parameters in discontinuous masonry structures has yet to be found in the literature.

Following this line, the current paper presents an inverse problem for identifying the mechanical parameters of a masonry bridge and an ogival masonry vault using FemDem in combination with Genetic Algorithms (GA). Two FemDem parametric models will be developed, the first depending on elastic parameters for a masonry bridge and the second on elastic and contact parameters for a similar masonry ogival vault. Before applying the inverse bridge problem, a parametric study based on direct FemDem simulations is performed in Section 3.1 to analyze the influence of the elastic and contact parameters on the distribution of vertical displacements at the bridge top.

To check the FemDem capabilities for the direct cases, a preliminary validation towards an experimental case taken from the literature is presented in Section 2. The first inverse problem is studied in Section 3 and focuses on identifying the Young modulus, Poisson ratio, and density of a masonry bridge, already studied in [30] but for other objectives. This identification is formulated with an objective function constructed from the displacements measured at the bridge contour. In Section 4, the second inverse problem computes an ogival vault's contact parameters (friction, cohesion, penalty spring, and fracture energy). The objective function is now constructed in terms of internal stresses and kinetic energy, being able to discriminate between collapse due to two instability types or compression failure.

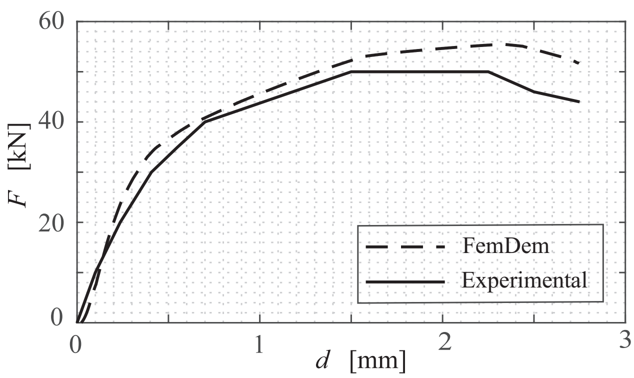


Figure 2: Numerical FemDem and experimental distributions for the TU Eindhoven wall. Displacement $d$ vs. reaction force $F$ at the top nodes

For both cases, the objective functions are minimized using a GA capable of finding the optimal parameters with a reduced number of cases. Due to the lack of experimental data in the first problem, the displacements on the bridge contour are calculated by direct FemDem simulations with a given set of predefined elastic parameters to be subsequently estimated by the GA. For the second case, a collection of safety coefficients and experimental limit loads of ogival vaults from [31] is used.

| $E$ | $\nu$ | $\mu$ | $\rho$ | $p_n$ | $p_t$ |
|---|---|---|---|---|---|
| [GPa] | [-] | [-] | [kg/m$^3$] | [GN/m] | [GN/m] |
| 16.7 | 0.15 | 0.75 | 2400 | 82 | 36 |

Table 1: Stone and equivalent mortar material properties for the shear wall of TU Eindhoven taken from [32]; user–chosen penalty parameters.

## 2. Eindhoven masonry wall

One of the common validations for DEM software is the TU Eindhoven experiment. A shear masonry wall of $1.08 \times 0.9$ [m] is studied in this section according to the indications of [32]. The wall is simplified to a 2D geometry with bricks of dimensions $220 \times 60$ [mm] in a running bond pattern. These bricks include two halves of the mortar thickness, and in turn, this mortar is simulated by a contact interface between bricks. The material properties for stone are Young modulus $E$ and Poison ratio $\nu$ are listed in Table 1; for mortar, they are friction coefficient $\mu$ and the numerical parameters normal and tangential penalties $p_n$, $p_t$.

A constant and vertical pressure of 0.8 [MPa] is applied to a top rigid beam, and its vertical position is locked; see Figure 1. Subsequently, a controlled horizontal displacement is induced in this beam, and the force necessary to apply is measured.

Figure 1 left shows the experimental crack, starting at the top right and running through the wall with an approximate angle of 45°. The crack obtained from the FemDem simulation of the central figure starts in the same position and follows a similar direction. The differences could be because, to save computer time, in FemDem the breakage of the bricks has not been activated. Finally, Figure 1 right shows the equivalent Tresca equivalent stresses (only inside blocks) that a similar wall without failure would have.

The force–displacement evolution is presented in Figure 2; the numerical and experimental results are very similar, confirming that the model reproduces reality well. The small difference at the end of the distribution, around 19% respect to the experiment, can be attributed to the mentioned impossibility of the brick breaking internally in the numerical model.

## 3. Masonry bridge with semicircular arch

In this section, a representative one–span masonry bridge is studied. The arch is semicircular with dimensions drawn in Figure 3, and it is discretized into 212 blocks with size $1 \times 0.5$ [m]. Most of the blocks in the walls are rectangular, but in the arch, they are slightly trapezoidal; by this arch, they are triangular, making the mesh continuous between the wall and arch as in real masonry structures. To prevent rigid body motions, the bridge is clamped at its base to simulate a strong foundation, and it is hinged at the sides to simulate the rest of the terrain. The blocks are internally divided into one to four finite elements with a total of 529; this additional discretization permits precise calculation of the elastic field. Most of the computational time is invested in iteratively solving the hundreds of contacts between blocks. Given that only initial collapses will be taken into account and to reduce the CPU time for contact, a map of possible contacts only among neighboring blocks has been implemented to reduce the search substantially.

The objective is to detect this structure's material and numerical parameters with the inverse problem. However, due to the lack of experimental data, a set of standard "real parameters" from the literature listed in Table 2 will be initially assigned. The parameters not already defined in Section 2 are cohesion $c$, fracture penalty $p_f$, energy fracture $G_f$, and tensile and shear strengths $f_t$, $f_s$ of the mortar.

| $E$ | $\nu$ | $\mu$ | $\rho$ | $p_n$ | $p_t$ |
|---|---|---|---|---|---|
| [GPa] | [-] | [-] | [kg/m$^3$] | [GN/m] | [GN/m] |
| 32 | 0.15 | 0.7 | 2500 | 298 | 30 |

| $c$ | $p_f$ | $G_f$ | $f_t$ | $f_s$ |
|---|---|---|---|---|
| [MPa] | [GN/m] | [MPa] | [MPa] | [MPa] |
| 6 | 14.1 | 8.5 | 210 | 780 |

Table 2: Mechanical properties of stone and mortar for the masonry bridge inverse problem.

### 3.1. Parametric analysis

A parametric analysis is carried out in this subsection to obtain a preliminary knowledge of the parameters' influence on the structural response, with initial values from Table 2 and ranges listed in the following figures' legends.

The influence of the elastic coefficients $E$ and $\nu$ on the vertical displacement $\Delta$ of the nodes at the top of the bridge is shown in Figure 4 a) and b) under the gravity force. As expected, $E$ has a strong influence on $\Delta$, with higher displacement for low values of $E$ and vice versa, see Figure 4 a). The influence of $\nu$ is unclear since large variations do not imply significant displacement changes. Again under gravity, $\nu$ mainly influences the blocks' horizontal displacement (not the vertical), which friction restricts. Only for the blocks close to the arch, $\Delta$ is important, and consequently, $\nu$ has a small overall influence in the vertical movement, see Figure 4 b).

Regarding the contact parameters, the penalties are slightly influential, as shown in Figure 5 c) and d). These are user–chosen and numerical (without physical meaning) variables, arbitrarily determined within recommended limits from [18]. Therefore, the inverse problem can help the user with the choice. The coefficient $\mu_f$ is more influential, Figure 5 bottom e), since it controls the relative displacement between blocks, and consequently, high values produce low displacements.

The fracture parameters $f_s$, $f_t$, $c$, $p_f$ and $G_f$ control the behavior of the mortar. Their variation does not significantly influ-

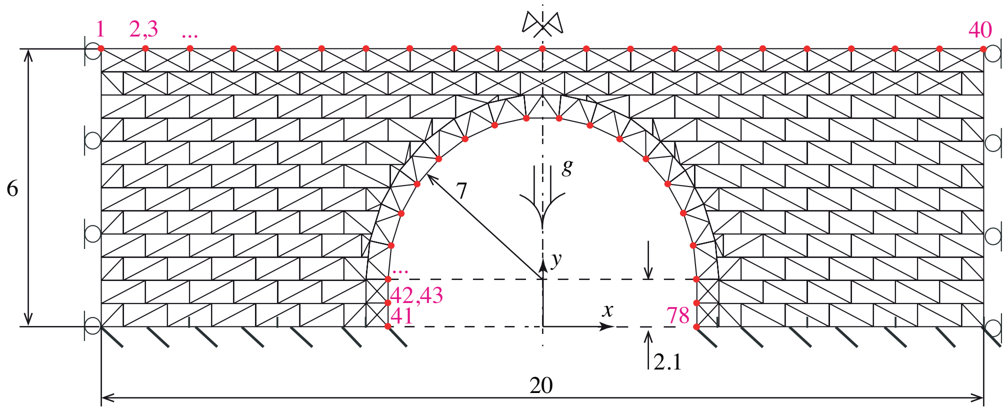


Figure 3: Boundary conditions, dimensions in [m] and FemDem mesh for a symmetric masonry bridge under gravity force. Red numbers represent the nodes for which displacements are measured; some are duplicated belonging to two adjacent bricks.

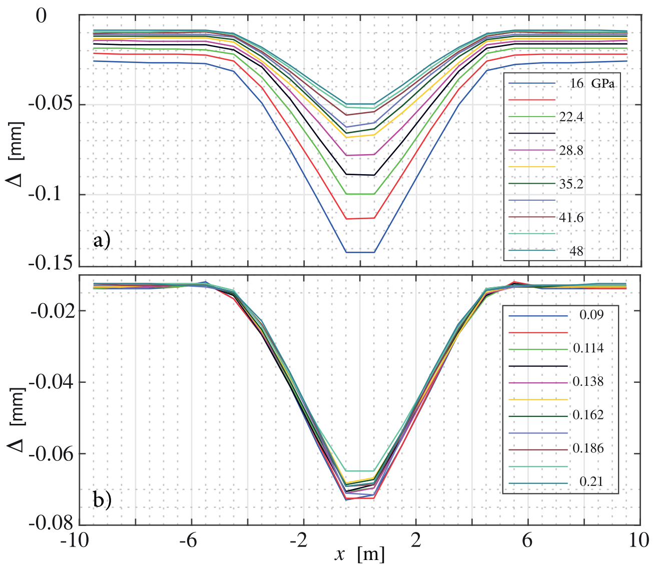


Figure 4: Vertical displacement at the bridge top of Figure 3, function of: a) Young moduli $E$ and b) Poison ratios $\nu$.

ence Δ since the current analysis is carried out for self–weight, and the stresses are far from failure. Therefore, these parameters will not be considered in this section, although they will be essential for cases in which cracks or other damages can occur (next section for ogival vault).

### 3.2. The objective function

The development of an inverse problem combining FemDem and GA is presented to find the elastic parameters and density automatically. The corresponding objective function $f_v$ is formulated with numerically calculated displacements, depending on three material parameters stored in the vector $\mathbf{X}^{GA}_{rnd} = \{E, \nu, \rho\}$.

As mentioned, since no in–situ measured data is available for this bridge, a set of numerical displacements obtained from the simulation of a direct FemDem case will be used instead of experimental displacements. These displacements are defined as vertical movements $\delta^{ex}_i$ at bridge top nodes ($i$ = 1 to 40) followed by arch intrados nodes ($i$ = 41 to 78) as plotted in Figure 6. The red dots depict the position and numbering of the nodes and numbers in Figure 3.

The inverse problem is handled in this work by GA, a heuristic optimization method that relies on the fundamental laws of genetics, [33]. In GA, the laws of natural selection are applied: superior members survive while inferior members are removed from a randomly generated population of individuals, commonly called chromosomes. The range of each variable is assigned by the user as will be done in Table 6. Among this population reside the possible solutions for optimal variables, and each possible one is evaluated with the objective function defined next. The evolution of subsequent populations is controlled by the genetic operators defined after Eq. 2. During this evolution, the children populations with the minimum objective functions replace some of their parent populations. The evolution continues until a cut–off criterion, the maximum amount of iterations, or a given tolerance is achieved.

To summarize the GA algorithm, the Figure 7 shows that with FemDem, a direct case using the real $\mathbf{X}$ of Table 3 is run from a single FemDem simulation, obtaining a displacement vector $\delta^{ex}_i$ with one entry for each control node $i$. These displacements will constantly be used for comparison, and to mimic the variations that always appear in experimental measurements, a random noise level of 5% is applied to the standard deviation of $\delta^{ex}_i$.

| Value | $E$ [GPa] | $\nu$ [-] | $\rho$ [$kg/m^3$] |
|---|---|---|---|
| Real | 32 | 0.15 | 2500 |
| Min, | 16 | 0.075 | 1250 |
| Max. | 64 | 0.2 | 5000 |
| Optimal | 31.25 | 0.144 | 2437 |

Table 3: Real (initial) values, calculation intervals, and optimized GA results.

Also, with FemDem but with data $\mathbf{X}^{GA}_{rnd}$ taken from the GA population, a set of parameterized vectors $\delta^j_i$ is subsequently calculated. For each iteration $j$, Eq. 1 defines the estimation of the objective function, formulated as the difference between the

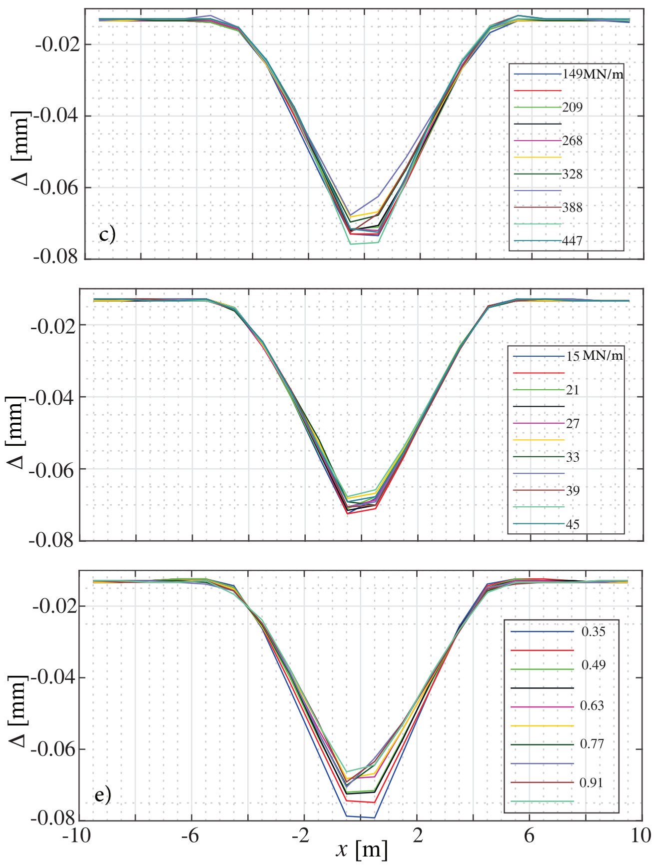


Figure 5: Vertical displacement at the bridge top of Figure 3, function of penalty parameters: c) normal $p_n$, d) tangential $p_t$, and e) friction coefficient $\mu_f$.

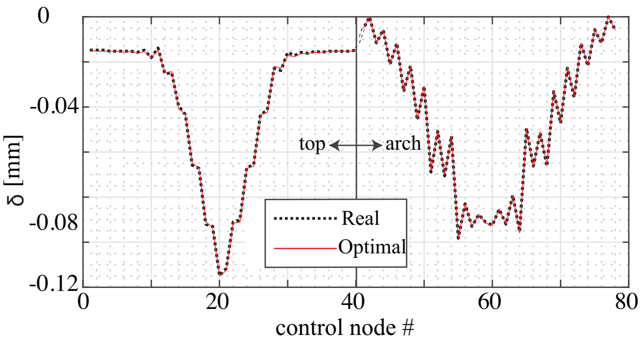


Figure 6: Vertical displacement distributions $\delta$ at the control nodes of Figure 3 for the $E$, $\rho$ and $\nu$ real and optimal values of Table 3.

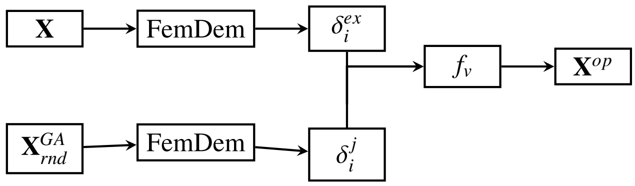


Figure 7: Flowchart for the computation of objective function and optimal values.

two displacement vectors.

$$f = \sum_{i=1}^{78} \left| \left( \delta_i^{ex} - \delta_i^j \right) \right| \tag{1}$$

The objective function is usually modified to $f_v = \log(f + \epsilon)$, where $\epsilon$ is a small dimensionless number here adopted as $\epsilon = 10^{-16}$. This value guarantees the existence of $f_v$ when $f$ approaches zero and enhances the convergence as explained in [34].

The inverse problem to identify the "real parameters" can be stated as a constrained minimization defined as finding a set $\mathbf{X}^{op}$ that achieves:

$$\min_{\mathbf{X}^{op}} \; f_v(\mathbf{X}_{rnd}^{GA}) \tag{2}$$

The evolution of $f_v$ (also called fitness value), along with the generations and the main parameters of the algorithm, are controlled by the user–chosen operators:

1. `population size`: number of seeds at initial iteration $j$ = 1, that is, of cases dependent on $\mathbf{X}_{rnd}^{GA}$.
2. `crossover fraction`: an operator to combine the genetic information from two parents to generate new descendants. It defines the maximum percentage that the $\mathbf{X}$ values are changed at each $j$.
3. `migration factor`: specifies the population fraction that moves to the new population. Only 20% (for the bridge case) of the bests in population $j$ move to the new $j + 1$.

As many values of $f_v$ as the population size are calculated, the best value is the minimum of $f_v$, and the mean value is its average.

### 3.3. Identification of parameters E, ν and ρ

Section 3.1 found that the only parameters that significantly influence the mechanical behavior of the bridge under self–weight are $E$ and $\nu$, but to complete the optimization, the density $\rho$ is added. This material property has not been considered in the parametric analyses since it is evident that in a structure under gravity, the higher the density, the higher the displacements. The evaluation of the three parameters with GA is studied in this section.

The GA algorithm designs an evolving population, and when the minimum of Eq. 2 is reached, the solution $\mathbf{X}^{op}$ is assigned to the current $\mathbf{X}_{rnd}^{GA}$ listed in the last row of Table 3 with a maximum error of 4% for $\nu$. The initial (named "real") and assumed intervals of the three parameters are also given in the table.

Figure 8 shows the convergence of the mean and best $f_v$ when the generations advance. It can be appreciated that at around generation 36, the calculation converged. Finally, a comparison between the initial and converged displacements is plotted in Figure 6, being the differences minimal since the real and optimized parameters are very similar, as mentioned.

## 4. Buried ogival vault

The buried ogival vault sketched in Figure 9 is analyzed in this section. To facilitate collapse, the vault has a thin, angu-

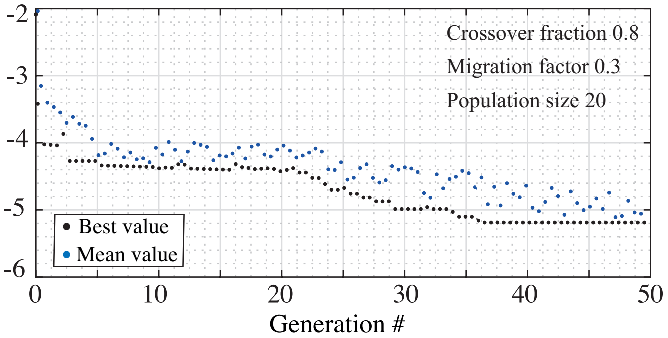


Figure 8: Generation vs. fitness value for the optimization of $\{E, \nu, \rho\}$. Mean and best fitness value.

lar opening of 20$^o$ at its peak; its width at the base is 15 [m], the height 8 [m], and the thickness is variable from 0.5 at the peak to 1 [m] at the base; the supports are clamped. Experimental stability results are taken from [31], and a detailed analysis computed by a refined version of the Discontinuous Deformation Analysis method is available in [17]. In this article, the basic stone and mortar parameters were approximately found by trial and error, not automatically like the present inverse problem does.

The vault is discretized into only 16 blocks to preserve the structure's geometry. This vault is subjected to self–weight, to a vertical distributed force $q_v$ from an embankment of variable height $h_e$ plus the effect of the related backfill, and to a lateral thrust $q_h$ of the backfill with fixed height $H = 8$ [m].

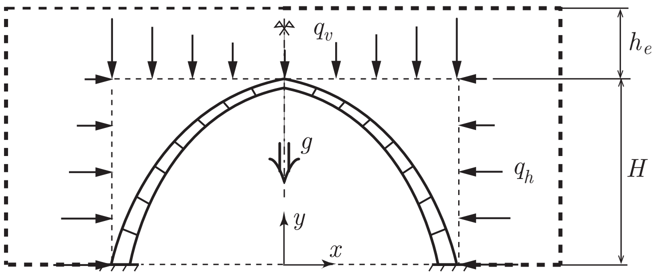


Figure 9: Buried ogival vault with variable embankment height $h_e$ and equivalent vertical and horizontal forces from Eqs. 3.

The expressions of these loads with $g$ the gravity acceleration are from basic formulae of Soil Mechanics:

$$\begin{aligned} q_v(y) &= h_e\, g\, \gamma_e + (H - y)\, g\, \gamma_f \\ q_h(y) &= \left(1 - \sin\phi_f\right)\, q_v(y) \end{aligned} \tag{3}$$

According to [17], the blocks are considered high strength and stiffness; see the last three columns of Table 4, with the specific weight $\gamma_s$ also listed. The backfill is gravel with specific weight $\gamma_f$ and friction angle $\phi_f$. It is considered that the embankment is made out of the same gravel but well compacted; consequently, an increase of 10% in its specific weight $\gamma_e$ is adopted. Additional mechanical and numerical properties related to contact and mortar will be defined in Section 4.1.

The experimental data used to compute the parameters is the collapse modes with their related limit loads. This collapse

| $\gamma_s$ | $\gamma_f$ | $\gamma_e$ | $\phi_f$ | $E$ | $\nu$ | $\sigma_u$ |
|---|---|---|---|---|---|---|
| [kg/m$^3$] | [kg/m$^3$] | [kg/m$^3$] | [°] | [GPa] | [-] | [MPa] |
| 2300 | 1600 | 1760 | 30 | 32 | 0.15 | 10 |

Table 4: Main mechanical properties of stone and backfill for the ogival vault.

can happen for three reasons, with respective zones separated in Figure 12:

- For low $h_e < 0.32$ [m], the horizontal $q_h$ dominates over the vertical $q_v$. The collapse produces the elevation of the peak, zone I.
- For intermediate $1.55 < h_e < 3.2$ [m], the arch is, in principle, stable. However, the collapse occurs by breakage of the blocks under compression, zone II.
- For high $h_e > 12.1$ [m], $q_v$ dominates over $q_h$. The collapse is produced by the descent of the peak, zone III.

Any embankment height between the maximum and minimum $h_e$ implies stability unless $h_e$ is intermediate. The Safety Factor (SF) is then defined as the number to multiply $h_e$ so that the induced $q_v$, $q_h$ provoke failure.

### 4.1. *Definition of the objective function*

The mentioned experimental factors SF from [31] are used as real data to define the objective function. But the reference does not include the values of the basic material coefficients. Therefore, the parameters to be optimized are related with contact between blocks $p_n$, $p_t$, $\mu$, and $c$, and with mortar $p_f$ and $G_f$.

Since there are six parameters to optimize, six experimental data $i$ must be considered to define the objective function. In turn and to establish the control of GA, each piece of data is defined by four parameters:

1. Safety factor SF in Figure 12 ordinate.
2. Height of the embankment $h_e$ in the abscissa.
3. Condition type: `type` = 0 indicates zones I or III (stability or instability), and `type` = 1 indicates zone II (block cracking or intact).
4. Condition satisfied: `fulfil` = 1 implies failure; `fulfil` = 0 implies intact structure.

Therefore:

- If `type` = 0, `fulfil` = 0 the vault is stable.
- If `type` = 0, `fulfil` = 1 the vault is unstable.
- If `type` = 1, `fulfil` = 0 the stone is not cracked.
- If `type` = 1, `fulfil` = 1 the stone is cracked.

Table 5 summarizes the experimental data and corresponding conditions. The first row $i = 1$ represents the minimum embankment height for a stable vault: for it, `type` = 0, and since the arch must be stable `fulfil` = 0. A decrease of this $h_e$

produces instability due to the horizontal thrust, as in the collapse sketch at the bottom–left, zone I of Figure 12. The data from the second and third rows are in zone II (breakage, `type` = 1). Two safety factors are forced for the same $h_e$ with unbroken stone, $i$ = 2 and `fulfil` = 0, and broken stone $i$ = 3 and `fulfil` = 1. These two conditions will help the GA to find optimum parameters with an intermediate and experimental SF = 3.77. A similar situation occurs for $h_e$ = 6.81 [m] in zone III, rows $i$ = 4, 5. For $i$ = 6, the vault becomes unstable again for $h_e$ = 12.06 [m] due to the high vertical load, as depicted in the collapse sketch at the bottom–right, zone III of Figure 12. In this situation, `type` = 0, and the arch must be unstable `fulfil` = 1.

| $i$ | SF | $h_e$ | `type` | `fulfil` |
|---|---|---|---|---|
| 1 | 1.00 | 0.33 | 0 | 0 |
| 2 | 3.75 | 2.00 | 1 | 0 |
| 3 | 3.80 | 2.00 | 1 | 1 |
| 4 | 1.85 | 6.81 | 0 | 1 |
| 5 | 1.88 | 6.81 | 0 | 0 |
| 6 | 1.00 | 12.06 | 0 | 0 |

Table 5: Safety factor SF, height of embankment $h_e$, type of condition and fulfilment for every $i$–condition.

For each GA iteration $j$, six simulations corresponding to the conditions of Table 5 (pairs of SF and $h_e$) are run. Once the six are completed, the outputs are post–processed according to Figure 10 flowchart, finishing the calculation with the variable `out`.

In this diagram, to distinguish between stable and unstable situations, the total kinetic energy $E_c$ of the 16 blocks is computed with FemDem. According to previous direct simulations, values of $E_c$ lower than 10 [J] imply stability: then `fulfil` = 0 and `out` = 0. If there is no stability, `out` is set to $E_c$ multiplied by a scaling factor: `out` = $E_c \cdot 10^{-11}$. The main purpose of this scaling is to achieve that all outputs have comparable orders of magnitude. The relevant variable for breakage conditions in zone II is the stress: for a broken stone `fulfil` = 1, the maximum stress $\sigma_{mx}$ in any block is greater than the maximum compressive stress $\sigma_u$, both in [MPa]. On the contrary, for non broken blocks `fulfil` = 0, $\sigma_{mx} < \sigma_u$. If the failure condition is met, the output variable `out` is set to 0, while if it is not, `out` is set to the difference between $\sigma_u$ and $\sigma_{mx}$ also scaled to obtain a similar order of magnitude to $E_c$.

Once the six simulations have been completed and all values of $\texttt{out}_i$ have been calculated, the objective function is defined as:

$$f_v = \log\left\{\left(\sum_{i=1}^{6} \texttt{out}_i\right) + 10^{-16}\right\} \tag{4}$$

In the previous equation, the logarithm function is applied to avoid zeros and numerical instabilities and the perturbation $10^{-16}$ to avoid values tending to $\infty$.

### 4.2. Identification of contact and mortar parameters

The experimental data from Table 5 are for instability and breakage; therefore, an inverse problem for identification of elastic and friction parameters as in Section 3.3 cannot be directly performed.

The stability parameters are defined at the beginning of Section 4.1, and their detection is studied in this section. Minimum and maximum values of these parameters are chosen from results of previous analyses and listed in Table 6; the range is wide since there is no clear idea of the final result. The GA randomly defines its population from this range and calculates the $f_v$ values according to the variable `out` of Figure 10. With it, the optimal values of the last row of the table are defined.

In Figure 11, the evolution of the GA algorithm is shown. For each iteration, the mean and best values of the population are plotted; it can be appreciated that the best value descends up to iteration 77 (dashed red line) when convergence is reached.

| | $p_n$ | $p_t$ | $\mu$ | $c$ | $p_f$ | $G_f$ |
|---|---|---|---|---|---|---|
| | | | [-] | [MPa] | | [N/m] |
| Min. | 11.93 | 1.19 | 0 | 1 | 1 | 1 |
| Max. | 596.3 | 59.7 | 2.5 | $10^4$ | $10^4$ | 20 |
| Opt. | 54.68 | 39.45 | 0.43 | 11.57 | 9.75 | 1.36 |

Table 6: Intervals and optimal values for the parameter identification of ogival vault. Penalty parameters $p$ in [MN/m].

The optimal results are within what is considered physical scope. The relevant penalty parameters $p_n$, $p_t$ are five and three times higher than those used in [17], meaning that a stronger constraint was needed in the contact algorithm. It is important to repeat that in this reference, the values were obtained by trial and error, then the possibility of employing inaccurate values was high. The friction is relatively low, confirming the assumption of the last reference; finally, the cohesion parameter is very low, probably because the masonry is dry without mortar between blocks.

### 4.3. Optimal parameters' experimental validation

A set of direct FemDem simulations is carried out to validate the calculated optimal parameters to reproduce the experimental data from [31]. First, the conditions from Table 5 are directly inserted in Figure 12. Then, direct FemDem cases with the optimal parameters of the table are run iteratively, incrementing the loads $q_v$ and $q_h$ until collapse is reached; the ultimate loads define SF. The figure shows the evolution of these SF that perfectly fit the experimental curve; consequently, the GA can be considered to have converged correctly. The numerical distribution shows that the optimized variables are valid for all embankment heights, even with relatively few conditions applied.

An additional direct case using the optimal parameters of Table 6 is studied for the same vault but under different loading conditions: a small and constant $h_e$ = 0.2 [m] and a point load in the range $F \in [0,180]$ [kN] applied at the peak. Figure 13 compares the SF evolution versus $F$ for experimental and FemDem data. A good agreement between both results is observed again despite being a different case. Therefore, using FemDem plus GA to obtain characteristic parameters can be considered satisfactory.

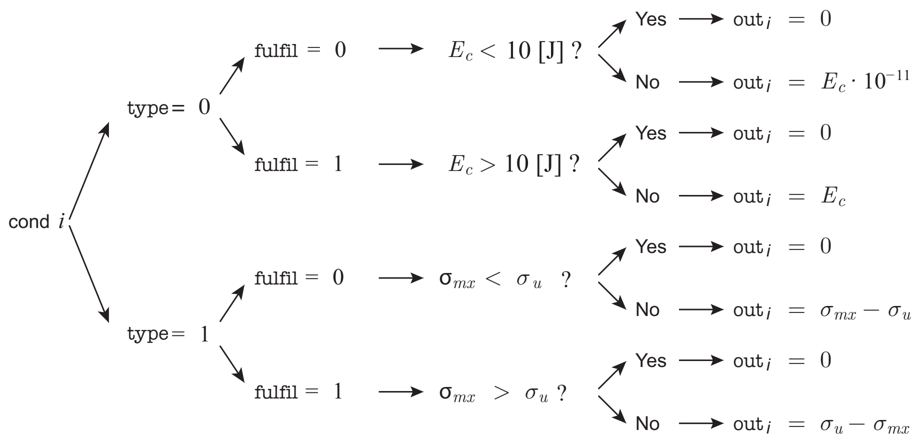


Figure 10: Flowchart for every condition with kinetic energy and ultimate stress criteria.

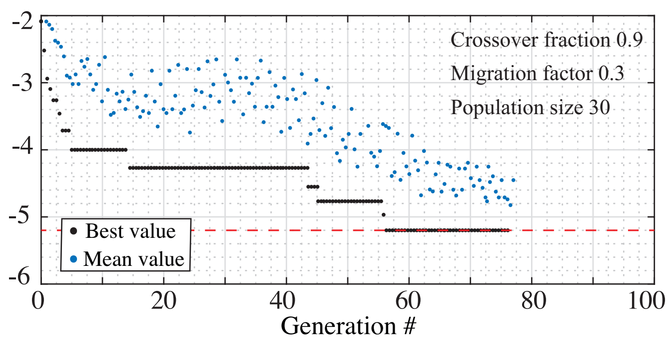


Figure 11: Evolution of the fitness value as a function of the number of generations.

## 5. Conclusions

In the current paper, a complete numerical tool for parameter detection of masonry structures has been applied to two different ones. The main mechanical characteristic of these constructions is contact and friction between blocks; then, discontinuous element methods are necessary. In addition, each block can be subdivided into internal finite elements, incrementing the precision for calculating stresses. This combination is called the FemDem method.

First, a direct parametric study of a bridge helps discern the more relevant material and contact properties for calculating displacements. Starting from a direct run of FemDem, the output displacements are modified with noise (as real experimental results always have), and they are used to detect the bridge's internal material and contact properties. A genetic algorithm for optimizing the number of cases helps the detection. The obtained properties are very similar to the initial ones, demonstrating the capability of the inverse problem to evaluate the future parameters of real bridges with some experimental data available.

Second, a few pieces of experimental global data are taken from the literature for a buried ogival vault and used again for parameter evaluation. These parameters are, in turn, applied to simulations of the same vault but under other loads, again fitting very well with the rest of the experimental results.

The current study has certain limitations, such as the high computational cost associated with structures containing numerous blocks or finely discretized blocks representing internal fractures. The numerical parameters (penalties) should not be directly applied to other structures and must be adjusted accordingly. In addition, prior knowledge of the mechanical behavior of the structure is required.

## Acknowledgements

This investigation has been developed in the framework of an ongoing research project: **Grant RTI2018-093621-B-I00**, "Simulación integrada no lineal del comportamiento estructural de puentes ferroviarios de fábrica ante acciones dinámicas y nuevos requerimientos de tráfico", funded by **MCIN/AEI/ - 10.13039/501100011033** and by **ERDF A way of making Europe**. The authors want to express their gratitude to the financial support provided by the aforementioned entities.

## References

[1] M. E. Rahman, Masonry Arch Bridge: Analysis & Assessment, Lap Lambert Academic Publishing, 2011.

[2] J. Hasley, Railway Masonry and Bridge Foundations, Railway age publishing, 1883.
URL `https://books.google.es/books?id=h3Y5AAAAMAAJ`

[3] J. Bien, L. Elfgren, J. Olofsson, Sustainable Bridges. Assessment for Future Traffic Demands and Longer Lives, Dolnoslaskie Wydawnictwo Edukacyjne, 2007.

[4] V. Pollio, H. Warren, M. Morgan, The Ten Books on Architecture, Harvard University Press, 1914.
URL `https://books.google.es/books?id=La4aAAAAYAAJ`

[5] F. J. Suarez, R. Bravo, Historical and probabilistic structural analysis of the royal ditch aqueduct in the alhambra (granada), Journal of Cultural Heritage 15 (5) (2014) 499–510. doi:https://doi.org/10.1016/j.culher.2013.11.010.

[6] U. C. 778-3R, Recommendations for the assessment of the load carrying capacity of existing masonry and mass-concrete arch bridge, Tech. rep., International Union of Railways (1994).

[7] Y.-L. Pi, N. Trahair, Three-dimensional nonlinear analysis of elastic arches, Engineering Structures 18 (1) (1996) 49–63. doi:10.1016/0141-0296(95)00039-3.

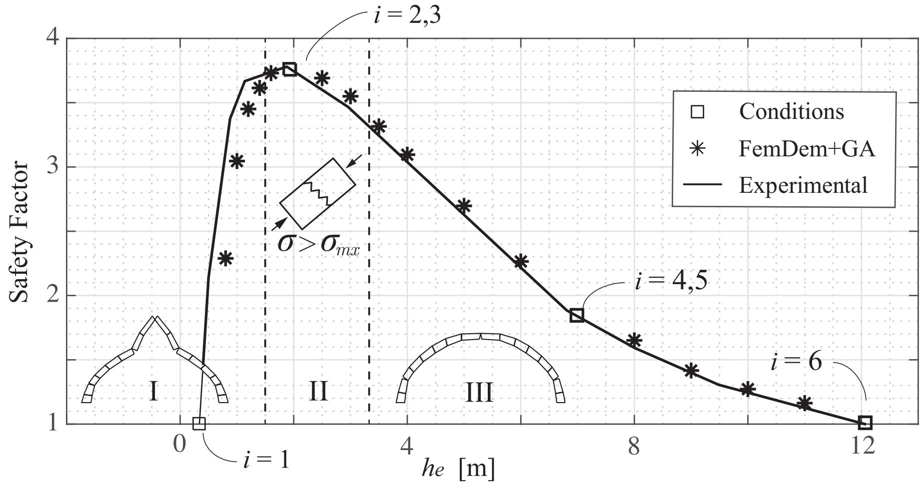


Figure 12: For ogival vault, SF vs. embankment height for experimental and numerical FemDem. Points inside curve: stability or intact; outside instability or cracking. Experimental conditions from Table 5 indicated by squares.

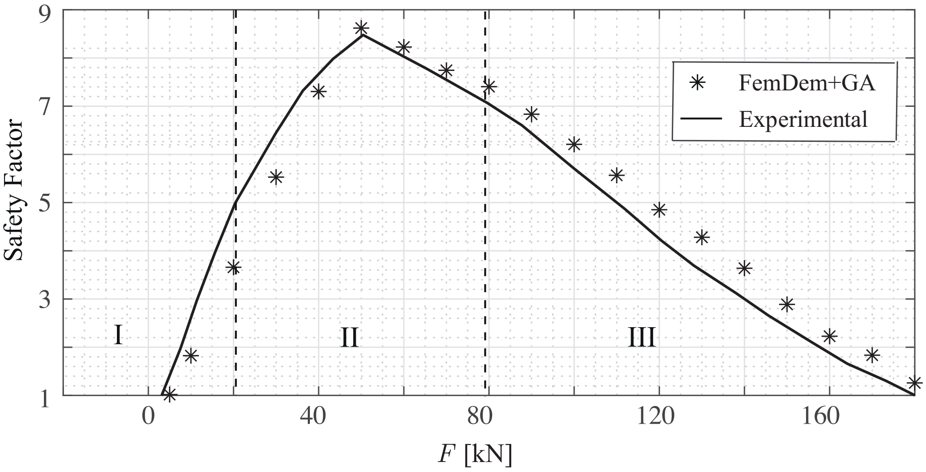


Figure 13: For ogival vault, SF vs. point load $F$ at the peak for experimental and numerical FemDem.


[8] P. Cundall, O. Strack, A discrete numerical model for granular assemblies, Geotechnique 29 (1979) 47–65.

[9] R. Bravo, J. L. Perez-Aparicio, Discontinuous numerical analysis of masonry vaults, Vol. 3, Springer-Verlag Berlin, Berlin, 2007, pp. 365–380.

[10] F. Gobbin, G. de Felice, J. V. Lemos, Numerical procedures for the analysis of collapse mechanisms of masonry structures using discrete element modelling, Engineering Structures 246 (2021) 113047. doi:https://doi.org/10.1016/j.engstruct.2021.113047.
URL `https://www.sciencedirect.com/science/article/pii/S014102962101186X`

[11] B. Pulatsu, E. Erdogmus, P. B. Lourenço, Simulation of masonry arch bridges using 3d discrete element modeling, in: R. Aguilar, D. Torrealva, S. Moreira, M. A. Pando, L. F. Ramos (Eds.), Structural Analysis of Historical Constructions, Springer International Publishing, Cham, 2019, pp. 871–880.

[12] F. J. Suárez, R. Bravo, J. A. González, Structural and constructive analysis of a faux vault, the dome of san juan de dios church, in granada (spain), International Journal of Architectural Heritage 15 (5) (2021) 728–739. doi:10.1080/15583058.2019.1645242.

[13] N. Bianchini, N. Mendes, C. Calderini, P. B. Lourenço, Modelling of the dynamic response of a reduced scale dry joints groin vault, Journal of Building Engineering 66 (2023) 105826. doi:https://doi.org/10.1016/j.jobe.2023.105826.
URL `https://www.sciencedirect.com/science/article/pii/S2352710223000050`

[14] F. Vadalà, V. Cusmano, M. F. Funari, I. Caliò, P. B. Lourenço, On the use of a mesoscale masonry pattern representation in discrete macro-element approach, Journal of Building Engineering 50 (2022) 104182. doi:https://doi.org/10.1016/j.jobe.2022.104182.
URL `https://www.sciencedirect.com/science/article/pii/S2352710222001954`

[15] A. Rafiee, M. Vinches, Mechanical behaviour of a stone masonry bridge assessed using an implicit discrete element method, Engineering Structures 48 (2013) 739–749. doi:https://doi.org/10.1016/j.engstruct.2012.11.035.

[16] K. M. Dolatshahi, A. J. Aref, Two-dimensional computational framework of meso-scale rigid and line interface elements for masonry structures, Engineering Structures 33 (12) (2011) 3657 – 3667. doi:10.1016/j.engstruct.2011.07.030.

[17] J. Pérez-Aparicio, R. Bravo, P. Ortiz, Refined element discontinuous numerical analysis of dry-contact masonry arches, Engineering Structures 48 (2013) 578–587. doi:https://doi.org/10.1016/j.engstruct.2012.09.027.

[18] A. A. Munjiza, The combined finite-discrete element method, John Wiley & Sons, 2004.

[19] L. Sun, Q. Liu, A. Abdelaziz, X. Tang, G. Grasselli, Simulating the entire progressive failure process of rock slopes using the combined finite-discrete element method, Computers and Geotechnics 141 (2022) 104557. doi:https://doi.org/10.1016/j.compgeo.2021.104557.

[20] X. Chen, X. Wang, H. Wang, A. K. Agrawal, A. H. Chan, Y. Cheng, Simulating the failure of masonry walls subjected to support settlement with the combined finite-discrete element method, Journal of Building Engineering 43 (2021) 102558. doi:https://doi.org/10.1016/j.jobe.2021.102558.
URL https://www.sciencedirect.com/science/article/pii/S2352710221004162

[21] H. Smoljanović, N. Zivaljić, Z. Nikolić, A combined finite-discrete element analysis of dry stone masonry structures, Engineering Structures 52 (2013) 89–100. doi:https://doi.org/10.1016/j.engstruct.2013.02.010.
URL https://www.sciencedirect.com/science/article/pii/S0141029613000655

[22] I. Balic, N. Zivaljic, H. Smoljanovic, B. Trogrlic, , Structural Engineering and Mechanics 58 (2) (2016) 243 – 257, cited by: 6. doi:10.12989/sem.2016.58.2.243.
URL https://www.scopus.com/inward/record.uri?eid=2-s2.0-84963771922&doi=10.12989%2fsem.2016.58.2.243&partnerID=40&md5=78f8a8761763ebd32692367cfd089d20

[23] B. Pulatsu, S. Gonen, E. Erdogmus, P. B. Lourenço, J. V. Lemos, R. Prakash, In-plane structural performance of dry-joint stone masonry walls: A spatial and non-spatial stochastic discontinuum analysis, Engineering Structures 242 (2021) 112620. doi:https://doi.org/10.1016/j.engstruct.2021.112620.

[24] J. Dorji, T. Zahra, D. Thambiratnam, D. Lee, Strength assessment of old masonry arch bridges through moderate destructive testing methods, Construction and Building Materials 278 (2021) 122391. doi:https://doi.org/10.1016/j.conbuildmat.2021.122391.
URL https://www.sciencedirect.com/science/article/pii/S0950061821001513

[25] J. J. Moughty, J. R. Casas, A state of the art review of modal-based damage detection in bridges: Development, challenges, and solutions, Applied Sciences 7 (5) (2017). doi:10.3390/app7050510.

[26] N. Grillanda, G. Milani, S. Ghosh, B. Halani, M. Varma, Shm of a severely cracked masonry arch bridge in india: Experimental campaign and adaptive nurbs limit analysis numerical investigation, Construction and Building Materials 280 (2021) 122490. doi:https://doi.org/10.1016/j.conbuildmat.2021.122490.
URL https://www.sciencedirect.com/science/article/pii/S0950061821002506

[27] H. Q. Do, A. M. Aragón, D. L. Schott, A calibration framework for discrete element model parameters using genetic algorithms, Advanced Powder Technology 29 (6) (2018) 1393–1403. doi:https://doi.org/10.1016/j.apt.2018.03.001.

[28] X. Zhao, Q. Dong, X. Chen, Y. Xiao, D. Zheng, Fatigue damage numerical simulation of cement-treated base materials by discrete element method, Construction and Building Materials 276 (2021) 122142. doi:https://doi.org/10.1016/j.conbuildmat.2020.122142.
URL https://www.sciencedirect.com/science/article/pii/S0950061820341453

[29] J. L. Pérez-Aparicio, R. Bravo, J. J. Gómez-Hernández, Optimal numerical design of bucket elevators using discontinuous deformation analysis, Granular Matter 16 (4) (2014) 485–498.
URL https://doi.org/10.1007/s10035-014-0485-5

[30] J. Pérez-Aparicio, R. Bravo, Combined finite–discrete element methods and genetic algorithms for damage detection in masonry bridges, submitted to Advances in Engineering Software (submitted 2022).

[31] J. Delbecq, Analyse de la stabilité des voûtes en maçonnerie par le calcul à la rupture, Journal de Mécanique théorique et appliquée 1 (1) (1982).

[32] P. Lourenco, Computational strategy for masonry structures (01 1996).

[33] D. E. Goldberg, The design of innovation: Lessons from and for competent genetic algorithms, Vol. 1, Springer, 2002.

[34] R. Gallego, G. Rus, Identification of cracks and cavities using the topological sensitivity boundary integral equation, Computational Mechanics 33 (2) (2004) 154–163.
URL https://doi.org/10.1007/s00466-003-0514-4